Nanoscale

Accepted Manuscript

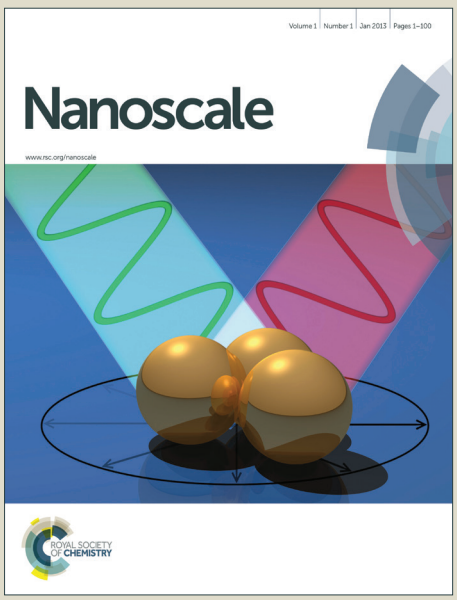

ROYAL SOCIETY OF CHEMISTRY

www.rsc.org/nanoscale

Journal Name

RSCPublishing

ARTICLE

Twin-Driven Thermoelectric Figure-Of-Merit Enhancement Of Bi_2Te_3 Nanowires

Cite this: DOI: 10.1039/x0xx00000x

Ho Sun Shin[a], Seong Gi Jeon[b], Jin Yu[b], Yong-Sung Kim[a,c], Hyun Min Park[a,c] and Jae Yong Song[a,c]*

Received 00th January 2012,
Accepted 00th January 2012

DOI: 10.1039/x0xx00000x

www.rsc.org/

Thermoelectric figure-of-merits (ZT) are enhanced or degraded by crystal defects such as twins and excess atoms that are correlated with thermal conductivity (k) and carrier concentration (n). For Bi_2Te_3, it is unclear whether the crystal defects can enhance ZT without a degradation in thermopower factor. In the present study, n-type Bi_2Te_3 nanowires (NWs) are electrochemically synthesized to have twin-free (TF) or twin-containing (TC) microstructures with ZT of 0.10 and 0.08, respectively, at 300 K. The ZTs of TF and TC NWs remarkably increase up to 0.21 and 0.31, when heat-treatments cause the n-reduction and twins induce the phonon scattering, as follows; first, the enhancement of Seebeck coefficient from -70 to -98 $\mu V \cdot K^{-1}$ for TF NW and -57 to -143 $\mu V \cdot K^{-1}$ for TC NW, by virtue of n-reduction; secondly, twin-driven k-reduction from 1.9 to 1.4 $W \cdot m^{-1} \cdot K^{-1}$ of TC NW, while the k of TF NW increases from 2.3 to 2.6 $W \cdot m^{-1} \cdot K^{-1}$ due to the enhanced carrier mobility. The lattice thermal conductivities of TC NW are lowered from 1.1 to 0.8 $W \cdot m^{-1} \cdot K^{-1}$ by phonon scattering at twins. And density functional theory calculations indicate that twins do not significantly influence the Seebeck coefficient of Bi_2Te_3. It is strongly recommended that twins be incorporated with an optimum carrier concentration to enhance the ZT of Bi_2Te_3.

1 Introduction

Thermoelectric (TE) materials have attracted great attention as promising candidates for clean and sustainable energy conversion. Among the TE materials, Bi_2Te_3 is the most efficient material near room temperature, because it has a high figure-of-merit, $ZT=(S^2\sigma)\cdot(kT)^{-1}$, of about 1 at room temperature, where S is the Seebeck coefficient, σ is electrical conductivity, k is thermal conductivity, and T is absolute temperature. Since it was theoretically predicted that ZT can be drastically enhanced by the size effect and quantum-confinement effect in nanostructures,[1] a plethora of studies have been made to fabricate Bi_2Te_3 nanostructures, such as nanowires (NWs),[2-7] superlattice films,[8] coaxial-superlattice NWs,[9,10] and nanotubes.[11,12] However, the Seebeck coefficients (-9 to -70 $\mu V \cdot K^{-1}$)[13-15] of Bi_2Te_3 NWs reported elsewhere were much smaller than those (-215 to -255 $\mu V \cdot K^{-1}$) of Bi_2Te_3 in the film and bulk forms near room temperature.[16-19] Even if the reasons have not been clearly understood, one possibility is the carrier concentration, which strongly influences the ZT of bulk Bi_2Te_3, according to the Pisarenko relation, i.e., thermopower decreases with an increase in carrier concentration.[20] The effects of carrier concentration on the Seebeck coefficient in nanowires have not been intensively investigated for Bi_2Te_3 NWs, although limited studies were recently reported for Bi_xTe_y, InAs, InSb NWs.[14,21]

Although the Wiedemann-Franz law, i.e., that electrical conductivity and thermal conductivity cannot be decoupled, limits ZT values, nanostructuring opens up the possibility that transport of phonons and electrons can be separately controlled by generating phonon scattering without significant degradation of electron mobility.[22,23] For example, internal defects such as superlattices, nanograins, and nanoprecipitates can increase ZT effectively through phonon scattering at the internal boundaries.[8,24,25] Recently, (001) basal twins were observed and analyzed in bulk Bi_2Te_3 by high-angle annular dark field (HAADF) scanning transmission electron microscopy (STEM) and a theoretical calculation.[26] The twin boundary, *i.e.* a well-ordered interface like a superlattice, is particularly interesting in view of the phonon-glass-electron-crystal, because electrical transport would be little affected by such interfaces where the phonon scattering occurs.[27] To the authors' knowledge, the effects of twins on the thermopower and lattice thermal conductivity of Bi_2Te_3 have not yet been investigated.

Hence, we synthesized twin-free and twin-containing Bi_2Te_3 NWs via a potentiostatic electrochemical method. The electrodeposition method, which has often been used to synthesize TE materials in the forms of thin films or NWs, can generate twins in metal deposits of Cu, Ag, Ni-Mn and Ag-Cu.[28-31] The effects of twins and carrier concentration on the TE properties of Bi_2Te_3 were experimentally and theoretically investigated using microfabricated TE measurement platform (MTMP) and density-functional theory (DFT) calculation.

2 Experimental Section

2.1 Synthesis of Bi_2Te_3 nanowires

Anodic aluminum oxide membrane (AAM) was prepared through a two-step anodization process at 274 K using aluminum

foils (99.99%, Alfa aesar).[32] After the anodization process, Au electrode layer (150 nm thick) was deposited on the AAM by RF sputtering deposition. The remaining aluminum was etched out in a mixed solution of 1 M $CuCl_2$ and 0.1 M HCl. The barrier layer of aluminum oxide was dissolved in 0.5 M phosphoric acid (323 K) for the electrodeposition process. The final pore size of AAM was approximately 55 nm in diameter. Electrochemical deposition was potentiostatically conducted at 298 K using a three-electrode setup composed of the Au-coated AAM as a working electrode, a saturated Ag/AgCl as a reference electrode, and a Pt wire as a counter electrode. The potential unit (V) versus a saturated Ag/AgCl electrode was used in this study. Cyclic voltammetry was performed to determine the reduction potential using a potentio/galvanostat (Solatron 1280c) at a scan rate of 20 $mV \cdot s^{-1}$. The aqueous electrolyte was composed of 0.004 M Bi^{3+} [$Bi(NO_3)_3$, Sigma-Aldrich, ACS grade], 0.004 M $HTeO^{2+}$ (TeO_2, Acros Organics), and 0.35 M HNO_3 (Junsei Chemical, GR grade). The pH of the electrolyte was 0.5. The reduction potentials (V_R) of +0.017 V and +0.120 V were used for the TF and the TC Bi_2Te_3 NWs, respectively. The nominal growth rate was estimated as 6.5 $\mu m \cdot h^{-1}$ at V_R of +0.017 V and 0.8 $\mu m \cdot h^{-1}$ at V_R of +0.120 V. The Bi_2Te_3 NWs within the AAM were heat-treated at 673 K for 2 hours in a vacuum (2 x 10^{-6} Torr).

2.2 Microstructural analyses

The morphology and length of the electrodeposited Bi_2Te_3 NWs in the AAM were investigated using a scanning electron microscopy (SEM, Hitachi, S4800). An atomic-scale microstructure analysis was conducted using aberration-corrected scanning transmission electron microscopy (CS-STEM, JEOL ARM200). For the sake of TEM analysis, the NWs-containing AAM was immersed in a 2 M NaOH aqueous solution to remove the AAM. Then, the NaOH solution was copiously rinsed out in deionized water and then ethanol. Finally, the NWs dispersed in ethanol were obtained after sonication for a few seconds. The NWs-containing ethanol was dropped onto a TEM grid and completely dried.

2.3 Measurement of TE properties

To characterize the thermopower factor of the Bi_2Te_3 NWs, we fabricated a membrane-type microfabricated TE measurement platform (MTMP) comprising a symmetric pair of Pt nanoheaters, current carrying electrodes, and four-point thermometers on a suspended low-stress silicon nitride of 500 nm thickness (Figure 1(a)). Ni/Al (10 nm/100 nm) layer was used as the electric and thermal contacts between Bi_2Te_3 NW and Pt electrode. The Pt thermometers had the electrical resistance of the two orders of magnitude smaller than the NWs. A temperature gradient was generated by resistive heating one of the Pt nanoheaters. The Seebeck voltage and electrical conductivity were measured under a vacuum (approximately 2 × 10^{-6} Torr) in the temperature range of 40 to 300 K. For the sake of measuring the thermal conductivity of NWs, we used a different micro-platform, *i.e.* suspended bridge-type MTMP (Figure 1(b)). As the heat generated from the nanoheater might be dissipated through the thin Si nitride (500 nm thick) bridges of the bridge-type MTMP, the measurements were conducted under the high vacuum. This enabled us to use one-dimensional heat conduction model ignoring thermal convection and thermal radiation.

2.4 Theoretical calculation

The TE properties of TF and TC Bi_2Te_3 were investigated by DFT calculations. Vienna Ab Initio Simulation Package (VASP) code was used.[33,34] We used the projector augmented wave (PAW) pseudopotentials.[35] The kinetic energy cutoff for the plane-wave

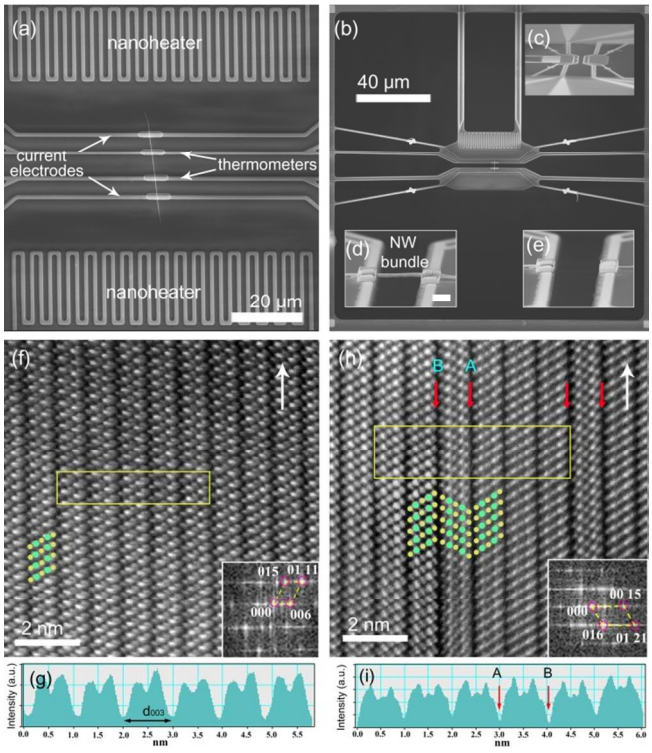

Figure 1. SEM images of (a) the membrane-type MTMP with a NW, (b) the bridge-type MTMP with NW bundle, (c) perspective view of the bridge-type MTMP, (d) suspended NW bundle bridging between hot and cold junctions, and (e) NW bundle after AFM cutting. HAADF-STEM results of (f) TF and (h) TC NWs. The atomic arrangement of Bi (bright) and Te (dark) atoms is distinguished by Z-contrast. (g) and (i) the atomic contrast profiles obtained from the yellow marked area of (f) and (h), respectively. The white arrows in (f) and (h) indicate the [110]-longitudinal growth direction of Bi_2Te_3 NWs. Twin boundaries are indicated by red arrows shown in (h). The insets in (f) and (h) indicate the FFT results of the corresponding HAADF-STEM images.

basis set expansion was 250 eV, and the generalized-gradient approximation (GGA) for the exchange correlation energy was used.[36] The spin-orbit coupling was included in the DFT Hamiltonian. The theoretical lattice constants of a=0.4478 nm and c=3.091 nm were used for the hexagonal three quintuple-layers unit cell (rhombohedral ($R\bar{3}m$) space group) of Bi_2Te_3 without twins. The 4×4×2 k-point mesh in the Brillouin zone for the three quintuple-layers unit cell was used for the geometry optimization and the total energy calculations. The Seebeck coefficients were calculated using the DFT band structures combined with the semiclassical theory of conduction under the energy-independent relaxation time approximation.[37] The 24×24×2 k-point mesh was used for the Seebeck coefficient calculation. With the theoretical lattice constants, the calculated electronic band structure has been known to agree well with the experiments.[38] The thickness of a quintuple layer (the distance between two nearby Van der Waals layers) is calculated to be 1.030 nm, whereas the experimentally obtained value is 1.036 nm, measured from HAADF image (Figure 1).

3 Results and discussion

The Seebeck coefficients (S) and the electrical conductivities (σ) of the Bi_2Te_3 NWs were measured using a membrane-type MTMP in the range of 40 to 300 K. Figure 1(a) shows a SEM image of the

membrane-type MTMP where a single Bi_2Te_3 NW was located on the four Pt electrodes in the center of the MTMP. In order to measure the thermal conductivity (k), we used a bridge-type MTMP, shown in Figs.1(b) and 1(c), which was similar to the previously reported method for measuring the thermal conductivity of Si NWs.[39] We used a Bi_2Te_3 NW bundle to measure the thermal conductivity because a single Bi_2Te_3 NW has too low thermal conductance to ensure measurement accuracy in our measurement system. Therefore, the thermal conductance of a single NW was averaged from that of the NW bundle. The thermal conductances of the NW bundle were determined by comparing the results obtained before and after cutting the Bi_2Te_3 bundle, respectively, as shown in Figs. 1(d) and 1(e). The detailed procedure of measuring S, σ and k is described in the method section (also see Supporting Information).

Bi_2Te_3 NWs with about 15 μm in length were electrochemically deposited into the anodic aluminum oxide membranes (AAMs) in potentiostatic mode by referring to the cyclic voltammogram (Figure S1). Two types of Bi_2Te_3 NWs were synthesized, to have twin-free (TF) and twin-containing (TC) microstructures at the reduction potential (V_R) of +0.017 and +0.120 V, respectively. The TF and TC NWs had diameters of 67±5 nm and 75±10 nm, respectively. Typical cross-sectional SEM images of the TF NWs and TC NWs showed that the NWs had smooth and void-free surfaces (Figures S2(a) and S2(c)). The bright-field TEM images of TF and TC NWs and the corresponding selected area electron diffraction (SAED) pattern for the whole nanowire showed that both Bi_2Te_3 NWs grew along the [110]-longitudinal direction (Figures S2(b) and S(d)). The TF NWs seemed to have almost single-crystalline structure, while the split diffraction pattern indicates that the TC NW was composed of several grains. The XRD results supported the stronger [110]-texturing along the longitudinal direction for TF NWs than TC NWs (Figure S3).

The HAADF-STEM images shown in Figures 1(f) and 1(h) indicate the quintuple atomic arrangements of the TF and TC NWs and the inset shows the corresponding fast Fourier transform (FFT) images. Figures 1(g) and 1(i) reflect the contrast profile for the marked area (yellow square) where the bright atoms (indicated by green color) represent the atomic columns of Bi atoms, while the dark ones (indicated by yellow color) correspond to the atomic columns of Te atoms. TF NW consisted of five repeating quintuple layers in the order of [-$Te^{(1)}$-Bi-$Te^{(2)}$-Bi-$Te^{(1)}$-] along the c-axis in a hexagonal structure (Rhombohedral ($R\bar{3}m$) space group). As the quintuple layers are weakly bonded to each other by Van der Waals force, it is shown that the repeating quintuple layers are widely separated by Van der Waals bonds (seen as dark stripes vertically appearing in the Figures 1(f) and 1(h)) between the $Te^{(1)}$ atomic layers. The distance between dark stripes was 1.036 nm, which agrees well with the (003) plane spacing of Bi_2Te_3.[40]

The HAADF-STEM image and corresponding FFT image of the TC NW clearly show that (001) basal twins (indicated by the red arrows) existed parallel to the longitudinal direction, as shown in

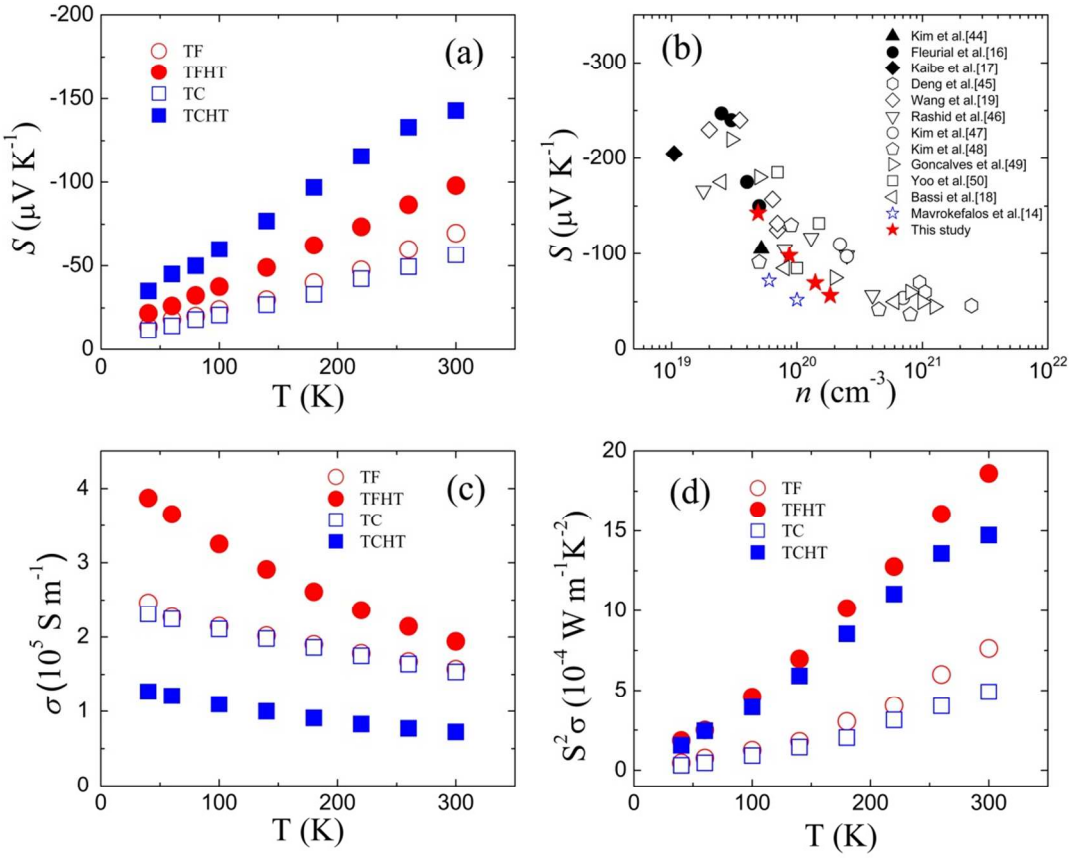

Figure 2.Variations of (a) Seebeck coefficients of Bi_2Te_3 NWs with temperature and (b) the Seebeck coefficients with carrier concentration for n-type Bi_2Te_3 including the literature data (solid symbols: bulk, open symbols: thin film, asterisk symbols: nanowire). Variations of (c) electrical conductivities and (d) thermopower factors of Bi_2Te_3 NWs with temperature. Here, TF, TFHT, TC, and TCHT denote twin-free, heat-treated twin-free, twin-containing, and heat-treated twin-containing NWs, respectively.

Figure 1(h). It was previously reported that the (001) basal twin terminated at the $Te^{(1)}$ layer in Bi_2Te_3 has the lowest interfacial energy among the possible twin structures.[26] Although the formation mechanism of twins in the NWs is not yet completely understood at the moment, the twin formation might be related to the electrodeposition parameters (e.g. reduction potential), as discussed in the references.[41,42] From the HAADF-STEM observation of six TC NWs, the number of twins was counted and the twin density was estimated to be approximately 1.2±0.9 twins per ten quintuples. And several stacking faults were locally found in both the TF and TC NWs.

Subsequently, the TF and TC NWs within the AAM were heat-treated at 673 K for 2 hours in a vacuum (2×10^{-6} Torr) and, hereafter, are termed TFHT and TCHT NWs, respectively. The microstructures of TFHT and TCHT NWs were not significantly changed after the heat-treatments. The single crystallinity of TFHT was maintained and the TCHT had similar twin-containing structure after the heat-treatment, as shown in the HADDF-STEM image and XRD data (Figures S4 and S5). This indicates that the present Bi_2Te_3 NWs had stable crystalline structure, which was different from the disproportionation (Bi_2Te_3 to Bi_4Te_3 *via* Bi_4Te_5) occurring due to Te sublimation in unstable Bi_2Te_3 crystalline structure.[4]

Figure 2(a) shows the variations of Seebeck coefficient over the temperature range of 40 to 300 K for TF, TC, TFHT, and TCHT NWs. The negative sign of the Seebeck coefficients indicates that all the NWs have *n*-type carriers. It is noted that the Seebeck coefficients linearly decreased with decreasing temperature, which was due to the contribution of diffusive thermopower rather than phonon drag effect.[43] At 300 K, the *S* (-70 $\mu V \cdot K^{-1}$) of TF NW, is comparable to the previous result (-70 $\mu V \cdot K^{-1}$ at 300 K) for the electrodeposited Bi_2Te_3 NWs,[14] but lower than that of Bi_2Te_3 thin films (-240 $\mu V \cdot K^{-1}$)[19] or bulk values (-250 $\mu V \cdot K^{-1}$).[16] And, it should be noted that the *S* (-57 $\mu V \cdot K^{-1}$) of TC NW was slightly smaller than that of TF NW. Therefore, we carried out a density functional theory (DFT) calculation in order to investigate the effects of twins on the thermopower of the Bi_2Te_3 phase. The twin density in our calculations was one twin per three quintuple layers. We found that lattice expansion of +0.55% occurred along the *c* axis with the twin insertion (Figure S6) and that the Te-Bi inter-layer spacing was barely changed, while the Te(1)-Te(1) Van der Walls inter-layer spacing was enlarged from 2.749 Å (TF Bi_2Te_3) to 2.896 Å (TC Bi_2Te_3) by +5.3%, which is in good agreement with the recent TEM measurement (+4.4%).[26] The calculated twin formation energy (the interface energy) was 22.7 $mJ \cdot m^{-2}$ per twin boundary, which was lower than the previous calculation (40.7 $mJ \cdot m^{-2}$).[26] According to the calculations of electronic density-of-states (DOS) and Seebeck coefficient (S) (at 300 K) of the TF and TC Bi_2Te_3 as a function of the Fermi level, the calculated *S* was +164 $\mu V \cdot K^{-1}$ (maximum value) in *p*-type and -156 $\mu V \cdot K^{-1}$ (maximum value) in *n*-type (see Figure S7), of which the absolute values were lower than those of the experimental values of +230 and -250 $\mu V \cdot K^{-1}$ (Figure S7).[16,18] For TC Bi_2Te_3, the calculated *S*'s were found to be lower, i.e., +129 $\mu V \cdot K^{-1}$ in *p*-type and -142 $\mu V \cdot K^{-1}$ in *n*-type. Approximately, 21% (*p*-type) and 9% (*n*-type) reductions of the *S*'s were found. The smaller gradients of the DOS at both the valence and conduction band edges for the TC Bi_2Te_3 might be ascribed to the smaller Seebeck coefficients. As a result, the calculation result (9% *S*-reductions of *n*-type) supports the measurement result of 19% *S*-reduction for TC NW.

However, according to the Pisarenko relation of *S* and carrier concentration (*n*) for highly-doped semiconductors,[20] the Seebeck coefficient is strongly affected by carrier concentration which is correlated to DOS. We estimated the carrier concentration of Bi_2Te_3 NWs using the linear relationship of S and T following the Mott formula,

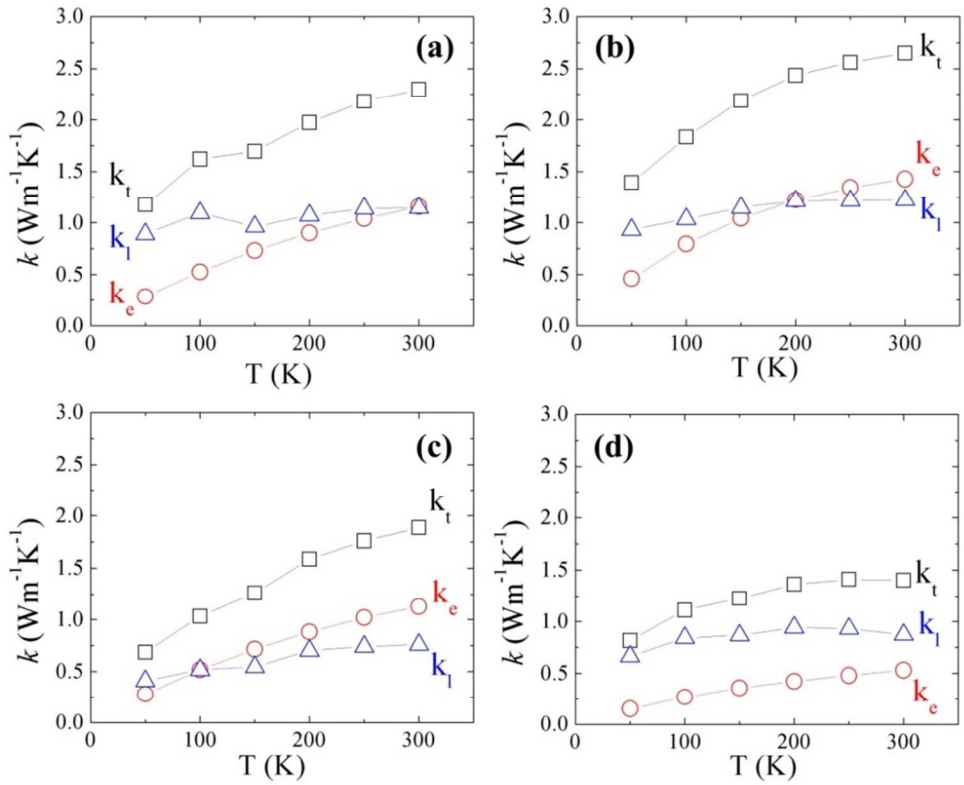

Figure 3. Variations of thermal conductivities of (a) TF, (b) TFHT, (c) TC, and (d) TCHT NWs with temperature. Open squares indicate the total thermal conductivity (kt), open circles the electronic thermal conductivity (ke), open triangles the lattice thermal conductivity (k_l)

$$\frac{S}{T} = -\frac{\pi^2 {k_B}^2 m^*}{(3\pi^2)^{2/3}\hbar^2|e|}\frac{1}{(n^{2/3})}$$

Under assumptions of a simple parabolic electronic band structure and a constant effective mass (m^*), the carrier concentrations were calculated as 1.4×10^{20} and 8.7×10^{19} cm^{-3} for TF and TFHT NWs while those of TC and TCHT NWs were estimated as 1.8×10^{20} and 4.9×10^{19} cm^{-3}, respectively. Here, $m^*=0.58m_0$ was used, where m_0 is electron rest mass.[20] Despite the similar carrier concentrations for TF and TC NWs, the TC NW had a lower S than the TF NW. This supports the premise that the lower S can be mainly attributed to the twin effect, as described by the above DFT calculation.

The carrier concentrations (n) of TF, TC, TFHT, and TCHT NWs were plotted with the previously reported results for Bi_2Te_3 film and bulk, as shown in Figure 2(b). It is noted that the S at room temperature decreased with the increasing n in the range of 10^{19} to 10^{21} cm^{-3}, indicating strong correlation between S and n.[14,16-19,44-50] The measured S for Bi_2Te_3 NWs agreed well with the S vs. n variations reported in the literature implying that the S of NWs might also be enhanced by optimization of n.

Figure 2(c) shows the variations of the electrical conductivities (σ) with temperature, and illustrates that all the NWs had increasing σ with decreasing temperature. This is presumed to be due to the increasing electron-phonon scattering with temperature. TF and TC NWs showed very similar σ variation (1.5×10^5 $S\cdot m^{-1}$ at 300 K). It is known that excess Te atoms occupying Bi sites play the role of n-type dopant and reduce the thermopower and mobility of Bi_2Te_3.[51]

Using the carrier concentrations (1.4×10^{20} and 1.8×10^{20} cm^{-3}), the carrier mobilities (μ) were calculated from the relation of $\sigma = nq\mu$, where q is electron charge. The μ (52 $cm^2\cdot V^{-1}\cdot s^{-1}$) of TC NW was slightly lower than that (70 $cm^2\cdot V^{-1}\cdot s^{-1}$) of TF NW (see Figure S8). The mobilities increased with decreasing temperature due to the diminishing scattering of carriers. The higher σ (1.94×10^5 $S\cdot m^{-1}$ at 300 K) of TFHT was due to the highly increased mobility, from 70 to 140 $cm^2\cdot V^{-1}\cdot s^{-1}$, despite the lowered carrier concentration, from 1.4×10^{20} to 8.7×10^{19} cm^{-3} after the heat-treatment, indicating that the lattice defects (e.g. anti-site defect) decreased and the crystallinity was enhanced by the heat-treatment. And the lower σ (0.59×10^5 Sm^{-1} at 300 K) of TCHT was ascribed to the decreased carrier concentration despite the small increase of mobility from 52 to 92 $cm^2\cdot V^{-1}\cdot s^{-1}$ (at 300 K) after the heat-treatment. The lower mobility of TCHT might be related to the carrier scattering at twin boundaries.

All gradients of μ vs. T increased in the sequence of TC, TF, TCHT, and TFHT, indicating that phonon scattering played an important role in decreasing μ with temperature for TFHT NW.

Figure 2(d) shows the variations of thermopower factor ($S^2\sigma$) with temperature, and that the $S^2\sigma$ increased after the heat-treatment; 7.6×10^{-4} to 18.6×10^{-4} $W\cdot m^{-1}\cdot K^{-2}$ for TFHT and 4.9×10^{-4} to 14.7×10^{-4} $W\cdot m^{-1}\cdot K^{-2}$ for TCHT. The improvement was due to the enhancement of Seebeck coefficient caused by the lowered carrier concentration of the heat-treated NWs.

We measured the thermal conductivity of the Bi_2Te_3 NWs by using the bridge-type MTMP shown in Figure 1(b). Practically, the thermal conductivity of Bi_2Te_3 NWs cannot be directly measured with a steady state method.[14,39] Rather, we measured the thermal conductance of NWs and converted it into thermal conductivity using the geometrical parameter (length and diameter) of the NWs provided by SEM observation. Considering the measurement reliability, we used a Bi_2Te_3 NW bundle composed of 5 to 6 NWs to enhance the sensitivity of measurement. To understand the effect of twinning on the lattice thermal conductivity (k_L) of NWs, we

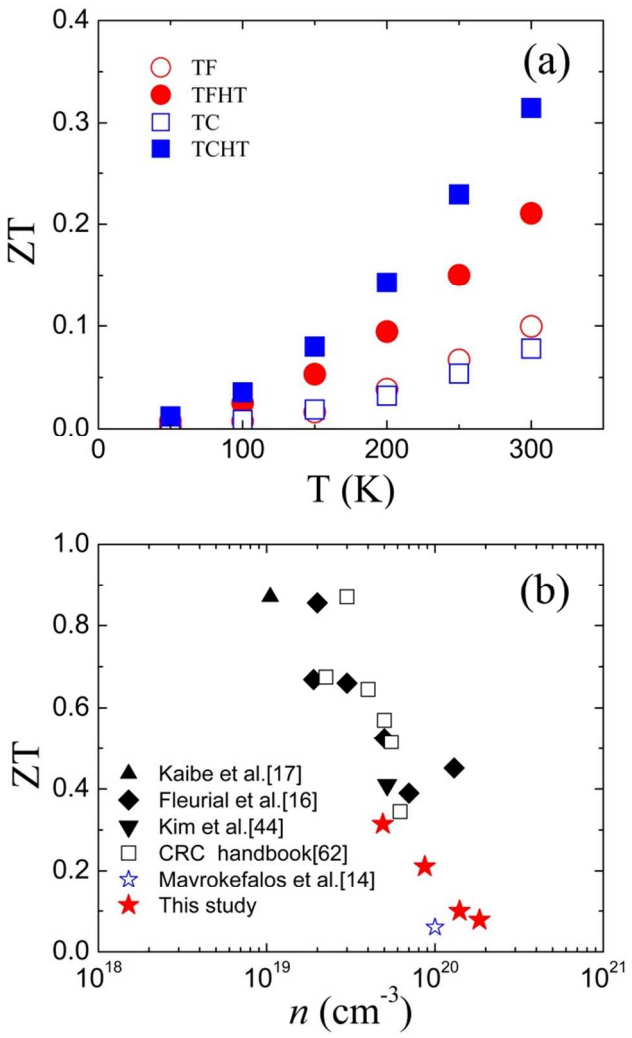

Figure 4. Variations of (a) ZTs of Bi_2Te_3 NWs with temperature and (b) the ZTs with the carrier concentration (n) of n-type Bi_2Te_3 including the literature data. (solid symbols: bulk, open symbols: thin film, asterisk symbols: nanowire). Here, TF, TFHT, TC, and TCHT denote twin-free, heat-treated twin-free, twin-containing, and heat-treated twin-containing, respectively.

extracted the electronic contribution (k_e) from the total thermal conductivity (k). The k_e was calculated by Wiedemann-Frantz law with the non-degenerated Lorentz number of 2.45×10^{-8} $W\cdot\Omega\cdot K^{-2}$ and electrical conductivity.[52] Here, the bipolar contribution to thermal conductivity was not considered because of the large contribution of electrons to thermal conductivity in highly n-doped Bi_2Te_3 NWs ($>10^{19}$ cm^{-3}).[53]

Figure 3 shows the k-variations of the Bi_2Te_3 NWs with temperature. At 300 K, the k of TF NW was measured to be 2.3 $W\cdot m^{-1}\cdot K^{-1}$, and of the TC NW to be 1.9 $W\cdot m^{-1}\cdot K^{-1}$. After the heat treatment at 673 K, TFHT showed the slightly increased k of 2.6 $W\cdot m^{-1}\cdot K^{-1}$, while TCHT exhibited the lowered k of 1.4 $W\cdot m^{-1}\cdot K^{-1}$ at 300 K. The k values of all NWs decreased with decreasing temperature; this was in contrast to the phenomena for the bulk sample, which shows increasing k with decreasing temperature. This implies that phonon-phonon umklapp scattering diminished while phonon-boundary and phonon–impurity scattering dominated in Bi_2Te_3 NWs.[54,55] In addition, although the electrodeposited Bi_2Te_3 NWs had a smooth surface apparently, they had an atomically rough surface, after heat treatment (Figure S4). The

rough surface serves as a strong phonon scattering site,[56] and even a phonon backscattering site.[57]

Generally, thermal conductivity is influenced by the microstructure and the carrier concentration. Mavrokefalos et al. reported that electrodeposited Bi_2Te_3 NWs had thermal conductivities (k) of 1 to 3 $W{\cdot}m^{-1}{\cdot}K^{-1}$ depending upon the microstructure and the carrier concentration.[10] In their study, the calculated k_e values were 0.35 and 1.51 $W{\cdot}m^{-1}{\cdot}K^{-1}$ for Bi_2Te_3 NWs with the carrier concentration of 6×10^{19} cm^{-3} and 1×10^{20} cm^{-3}, respectively. Chen et al. also reported the low k (0.75 $W{\cdot}m^{-1}{\cdot}K^{-1}$) of electrodeposited Bi_2Te_3 NWs with a [100]-preferred orientation in an amorphous alumina matrix,[13] but they did not investigate the effects of n on thermoelectric transport. Higher n leads to higher electrical conductivity, whereby the thermal conductivity will be increased by the increasing electronic component k_e. The calculated k_e (1.4 $W{\cdot}m^{-1}{\cdot}K^{-1}$) for TFHT increased in comparison with that (1.1 $W{\cdot}m^{-1}{\cdot}K^{-1}$) of TF despite the decreased n, while the k_e for TCHT decreased due to the decreased n. The increased k_e for TFHT was attributed to the increased μ (Figure S8). On the other hand, the decreased k_e for TCHT was due to a larger decrease of the n.

Regarding the k_L, we found that the k_L's for TC (0.8 $W{\cdot}m^{-1}{\cdot}K^{-1}$) and TCHT (0.9 $W{\cdot}m^{-1}{\cdot}K^{-1}$) were lower than those of TF (1.1 $W{\cdot}m^{-1}{\cdot}K^{-1}$) and TFHT (1.2 $W{\cdot}m^{-1}{\cdot}K^{-1}$). The k_L's were comparable to the other report in the literature that k_L varied depending upon the microstructure of NWs, i.e., k_L of 0.35 and 1.5 $W{\cdot}m^{-1}{\cdot}K^{-1}$ for single crystalline and polycrystalline Bi_2Te_3 NWs at 400 K, respectively.[10] And it was reported that the nanostructuration of Bi_2Te_3 nanowires (56 nm in diameter) with twins leads to a reduction in the speed of sound, predicting a 13%-reduction in the lattice thermal conductivity.[58] The 25%-lower k_L for TC and TCHT Bi_2Te_3 NWs might be related to the higher twin density, considering the similar NW diameters of 67 and 75 nm.

Introducing twins into TE materials has been considered to enhance the ZT by decreasing thermal conductivity by phonon scattering at twin boundaries. It was reported that thermal conductivity was depressed by twin boundaries in an indium-thallium alloying bulk.[59] Considering the higher twin density of TC and TCHT NWs, k_L reduction for TC by additional phonon scattering at twin boundaries can be expected. If the phonon scattering added by twins is independent of other sources, we can combine the phonon scattering rate of twins (τ_{twin}^{-1}) into the total phonon scattering rate(τ_{total}^{-1}) following Mathiessen's rule, as follows: $\tau_{total}^{-1} = \Sigma\tau_{other}^{-1} + \tau_{twin}^{-1}$, where τ_{other}^{-1} indicates other scattering process such as phonon-phonon scattering, phonon-point defect scattering, and phonon-boundary scattering. Assuming that the twins can effectively confine the phonon propagation within neighboring quintuple layers, the scattering rate at twins would significantly increase because the effective length scale of scattering is dominated by the interspacing between neighboring twins rather than the NW's diameter. Actually, for the twin density of one twin per ten quintuples, the interspacing between twins was approximately 10 nm. Previously, it was reported that a small confinement dimension below 10 nm would lead to a large suppression in the lattice thermal conductivity.[56,60,61] Thus, it is reasonably supposed that the lower k_L for TC can be mainly ascribed to the scattering at twins as well as the surface scattering.

The ZTs for the Bi_2Te_3 NWs are plotted with temperature in Figure 4(a). The ZT was calculated to be 0.10 for TF NW and 0.08 for TC NW at 300 K. Notably, after a heat treatment at 673 K, the TCHT had higher ZT (0.31) than that (0.21) of TFHT. In good agreement with the Pisarenko relation, the lower carrier concentration of TFHT and TCHT NWs leads to the higher Seebeck coefficient. In addition, the thermal conductivity lowered by twin scattering enabled TCHT to have the highest ZT among the present Bi_2Te_3 NWs. The ZTs for Bi_2Te_3 NWs are plotted with other literature data for Bi_2Te_3 film and bulk in Figure 4(b).[14,16,17,43,62] It is evident that ZT has a strong correlation to carrier concentration. This result implies that the Pisarenko relation still holds regardless of the dimension of TE materials and the maximum ZT of NWs can be obtained when the carrier concentration is carefully optimized.

4 Conclusions

Twin-free and twin-containing Bi_2Te_3 NWs were electrochemically synthesized by controlling the reduction potential, in order to investigate the effects of twins on TE properties. The TE properties of the synthesized Bi_2Te_3 NWs were characterized by using two types of microfabricated device (the membrane-type and the island-type MTMP) from 40 K to 300 K. The TCHT NW had the highest ZT of 0.31 due to enhanced Seebeck coefficient and lowered thermal conductivity despite lowered electrical conductivity. The enhanced ZT was mainly attributed to the reduction of the carrier concentration, which gives rise to increasing thermopower according to the Pisarenko relation. Although DFT calculations indicated a 9% S-degradation by twins in n-type Bi_2Te_3, the k_L-suppression by twins led to the ZT enhancement of Bi_2Te_3 NWs. The k_L was lowered for the twin-containing microstructure suggesting that twins effectively reduce the lattice thermal conductivity regardless of the carrier concentration.

According to the roundup of ZTs of Bi_2Te_3 thin films and bulk in the literature, the correlation between the carrier concentration and ZT is valid for Bi_2Te_3 NWs. That suggests that the ZT enhancement of NWs can be achieved by optimizing the carrier concentration and nanoengineering twins.

Acknowledgements

This work was supported by Future-based Technology Development Program (Nano Fields) through the National Research Foundation of Korea (NRF) funded by the Ministry of Education, Science and Technology (Grant No. 20120009623).

Notes

[a] *Center for Nanomaterials Characterization, Korea Research Institute of Standards and Science, Daejeon, 305-340, Republic of Korea. *E-mail: jysong@kriss.re.kr*

[b] *Department of Materials Science and Engineering, Korea Advanced Institute of Science and Technology, Daejeon 305-701, Republic of Korea.*

[c] *University of Science and Technology, Daejeon 305-350, Republic of Korea*

†Electronic Supplementary Information (ESI) available [Additional results on microstructural analysis, DFT calculation, carrier mobilities and procedure of measuring TE properties of NW]. See DOI: 10.1039/b000000x/.

References

1 L. D. Hicks, M. S. Dresselhaus, *Phys. Rev. B* 1993, **47**, 16631.

2 B. Hamdou, J. Kimling, A. Dorn, E. Pippel, R. Rostek, P. Woias, K. Nielsch, *Adv. Mater.* 2013, **25**, 239.

3 O. Picht, S. Müller, I. Alber, M. Rauber, J. Lensch-Falk, D. L. Medlin, R. Neumann, M. E. Toimil-Molares, *J. Phys. Chem. C* **2012**, 116, 5367.

4 J. Lee, A. Berger, L. Cagnon, U. Gosele, K. Nielsch, J. Lee, Phys. Chem. Chem. Phys. 2010, **12**, 15247.
5 J. Ham, W. Shim, D.H. Kim, S. Lee, J. Roh, S.W. Sohn, K.H. Oh, P.W. Voorhees, W. Lee, Nano Lett. 2009, **9**, 2867.
6 E.J. Menke, Q. Li, R.M. Penner, Nanolett., 2004, **4**, 2009.
7 M.S. Sander, A.L. Prieto, R. Gronsky, T. Sands, A.M. Stacy, Adv. Mater. 2002, **14**, 665.
8 R. Venkatasubramanian, E. Siivola, T. Colpitts, B. O'Quinn, *Nature* 2001, **413**, 597.
9 W. Wang, X. Lu, T. Zhang, G. Zhang, W. Jiang, X. Li, *J. Am. Chem. Soc.* 2007, **129**, 6702.
10 B. Yoo, F. Xiao, K. N. Bozhilov, J. Herman, M. A. Ryan, N. V. Myung, *Adv. Mater.* 2007, **19**, 296.
11 Z. Chai, Z. Peng, C. Wang, H. Zhang, *Mater. Chem. Phys.* 2009, **113**, 664.
12 G. Zhang, Q. Yu, Z. Yao, X. Li, *Chem. Comm.* 2009, 2317.
13 C.-L. Chen, Y.-Y. Chen, S.-J. Lin, J. C. Ho, P.-C. Lee, C.-D. Chen, S. R. Harutyunyan, *J. Phys. Chem. C* 2010, **114**, 3385.
14 A. Mavrokefalos, A. L. Moore, M. T. Pettes, L. Shi, W. Wang, X. Li, *J. Appl. Phys.* 2009, **105**, 104318.
15 J. Zhou, C. Jin, J. H. Seol, X. Li, L. Shi, *Appl. Phys. Lett.* 2005, **87**, 1.
16 J. P. Fleurial, L. Gailliard, R. Triboulet, H. Scherrer, S. Scherrer, *J. Phys.Chem. Solids* 1988, **49**, 1237.
17 H. Kaibe, Y. Tanaka, M. Sakata, I. Nishida, *J. Phys.Chem. Solids* 1989, **50**, 945.
18 A. Li Bassi, A. Bailini, C. S. Casari, F. Donati, A. Mantegazza, M. Passoni, V. Russo, C. E. Bottani, *J. Appl. Phys.* 2009, **105**, 124307.
19 X. Wang, H. He, N. Wang, , L. Miao, *Appl. Surf. Sci.* 2013, **276**, 539.
20 G. S. Nolas, J. Sharp, J. Goldsmid, *Thermoelectrics: Basic Principles and New Materials Developments*. Springer: 2001.
21 A. Soni, Z. Yanyuan, Y. Ligen, M. K. K. Aik, M. S. Dresselhaus, Q. Xiong, *Nano Lett.* 2012, **12**, 1203.
22 M. G. Kanatzidis, *Chem. Mater.* 2010, **22**, 648.
23 P. Pichanusakorn, P. Bandaru, *Mater. Sci. and Eng. R: Reports* 2010, **67**, 19.
24 S. K. Bux, R. G. Blair, P. K. Gogna, H. Lee, G. Chen, M. S. Dresselhaus, R. B. Kaner, J. P. Fleurial, *Adv. Funct. Mater.* 2009, **19**, 2445.
25 Y. Lan, B. Poudel, Y. Ma, D. Wang, M. S. Dresselhaus, G. Chen, Chen, Z. Ren, *Nano Lett.* 2009, **9**, 1419.
26 D. L. Medlin, Q. M. Ramasse, C. D. Spataru, N. Y. C. Yang, *J. Appl. Phys.* 2010, **108**, 043517
27 D. L. Medlin, G. J. Snyder, *Curr. Opin. Colloid and Interface Sci.* 2009, **14**, 226.
28 G. Lucadamo, D. L. Medlin, N. Y. C. Yang, J. J. Kelly, A. A. Talin,.*Phil. Mag*. 2005, **85**, 2549.
29 S. H. Park, H. S. Shin, Y. H. Kim, H. M. Park, J. Y. Song, .*Nanoscale* 2013, **5**, 1864.
30 S. H. Park, H. S. Shin, Y. H. Kim, H. M. Park, J. Y. Song, *J. Alloys & Comp.* 2013, **580**, 152.
31 S. Zhong, T. Koch, M. Wang, T. Scherer, S. Walheim, H. Hahn, T. Schimmel, *Small* 2009, **5**, 2265.
32 H. S. Shin, J. Yu, J. Y. Song, H. M. Park, *Appl. Phys. Lett.* 2009, **94**, 011906.
33 G. Kresse, J. Furthmüller, *Phys. Rev. B* 1996, **54**, 11169.
34 G. Kresse, D. Joubert, *Phys. Rev. B* 1999, **59**, 1758.
35 P. E. Blöchl, *Phys. Rev. B* 1994, **50**, 17953.
36 J. P. Perdew, J. A. Chevary, S. H. Vosko, K. A. Jackson, M. R. Pederson, D. J. Singh, C. Fiolhais, *Phys. Rev. B* 1992, **46**, 6671.
37 T. J. Scheidemantel, C. Ambrosch-Draxl, T. Thonhauser, J. V. Badding, J. O. Sofo, *Phys. Rev. B – Cond. Matt. Mater. Phys.* 2003, **68**, 1252101.
38 G. Wang, T. Cagin, *Phys. Rev. B* 2007, **76**, 075201.
39 A. I. Boukai, Y. Bunimovich, J. Tahir-Kheli, J.-K. Yu, W. A. Goddard Iii, J. R. Heath, *Nature* 2008, **451**, 168.
40 Joint Committee Powder Diffraction Standards (JCPDS) International center for diffraction data, PDF No. 15-0863, Swarthmore, PA 2003. for diffraction data, PDF No. 27-1402, Swarthmore, PA, 2003
41 V. M. Kozlov, L. *J.* Peraldo Bicelli, *Cryst. Growth* 1996, **165**, 421.
42 V. M. Kozlov, L. *J.* Peraldo Bicelli, *Cryst. Growth* 1997, **177**, 289.
43 F.J. Blatt, P.A. Schroeder, C.L. Foiles, D. Greig, Thermoelectric power of metals, Plenum press, NY 1976.
44 D. H. Kim, C. Kim, S. H. Heo, H. Kim, *Acta Mater.* 2011, **59**, 405.
45 Y. Deng, H.-M. Liang, Y. Wang, Z.-W. Zhang, M. Tan, J.-l. Cui, *J. Alloys & Comp.* 2011, **509**, 5683.
46 M. M. Rashid, K. H. Cho, G. S. Chung, *Appl. Surf. Sci.* 2013, **279**, 23.
47 M. Y. Kim, T. S. Oh, J. S. Kim, *J. Kor. Phys. Soc.* 2007, **50**, 670.
48 D. H. Kim, G. H. Lee, *Mater. Sci. Eng. B* 2006, **131**, 106.
49 L. M. Goncalves, C. Couto, P. Alpuim, A. G. Rolo, F. Völklein, J. H. Correia, *Thin Solid Films* 2010, **518**, 2816.
50 B. Y. Yoo, C. K. Huang, J. R. Lim, J. Herman, M. A. Ryan, J. P. Fleurial, N. V., Myung, *Electrochim. Acta* 2005, **50**, 4371.
51 S. Cho, Y. Kim, A. DiVenere, G. K. Wong, J. B. Ketterson, J. R. Meyer, *Appl. Phys. Lett.* 1999, **75**, 1401.
52 C. Kittel, *Introduction to solid state physics*. Wiley: 1996.
53 C. F. Gallo, B. S. Chandrasekhar, P. H. Sutter, *J. Appl. Phys.* 1963, **34**, 144.
54 D. Li, Y. Wu, P. Kim, L. Shi, P. Yang, A. Majumdar, *Appl. Phys. Lett.* 2003, **83**, 2934.
55 R. C. Zeller, R. O. Pohl, *Phys. Rev.B* 1971, **4**, 2029.
56 B. Qiu, , L. Sun, X. Ruan, *Phys. Rev. B* 2011, **83**, 035312.
57 A. L. Moore, S. K. Saha, R. S. Prasher, L. Shi, *Appl. Phys. Lett.* 2008, **93**, 083112.
58 D. Bessas, W. Töllner, Z. Aabdin, N. Peranio, I. Sergueev, H. Wille, O. Eibl, K. Nielsch, R. P. Hermann, *Nanoscale* 2013, **5**, 10629.
59 L. S. Mitchell, A. C. Anderson, *J. Low. Temp. Phys.* 1993, **91**, 341.
60 A. L. Moore, M. T. Pettes, F. Zhou, L. Shi, *J. Appl. Phys.* 2009, **106**, 034310.
61 S. G. Walkauskas, D. A. Broido, K. Kempa, T. L. Reinecke, *J. Appl. Phys.* 1999, **85**, 2579.
62 D. M. Rowe, *Thermoelectrics Handbook: Macro to Nano*. Taylor & Francis: 2010.